Article

Humans in Africa's wet tropical forests 150 thousand years ago

https://doi.org/10.1038/s41586-025-08613-y

Received: 16 February 2024

Accepted: 8 January 2025

Published online: 26 February 2025

Open access

Check for updates

Eslem Ben Arous[1,2,3]✉, James A. Blinkhorn[2,4]✉, Sarah Elliott[5], Christopher A. Kiahtipes[6], Charles D. N'zi[7], Mark D. Bateman[8], Mathieu Duval[1,9,10], Patrick Roberts[11,12,13], Robert Patalano[11,14], Alexander F. Blackwood[2,10,15], Khady Niang[2,16], Eugénie Affoua Kouamé[17], Edith Lebato[7], Emily Hallett[18], Jacopo N. Cerasoni[19], Erin Scott[11,12], Jana Ilgner[11], Maria Jesús Alonso Escarza[1], Francois Yodé Guédé[7] & Eleanor M. L. Scerri[2,13,20]✉

Humans emerged across Africa shortly before 300 thousand years ago (ka)[1–3]. Although this pan-African evolutionary process implicates diverse environments in the human story, the role of tropical forests remains poorly understood. Here we report a clear association between late Middle Pleistocene material culture and a wet tropical forest in southern Côte d'Ivoire, a region of present-day rainforest. Twinned optically stimulated luminescence and electron spin resonance dating methods constrain the onset of human occupations at Bété I to around 150 ka, linking them with *Homo sapiens*. Plant wax biomarker, stable isotope, phytolith and pollen analyses of associated sediments all point to a wet forest environment. The results represent the oldest yet known clear association between humans and this habitat type. The secure attribution of stone tool assemblages with the wet forest environment demonstrates that Africa's forests were not a major ecological barrier for *H. sapiens* as early as around 150 ka.

Our species (*Homo sapiens*) is thought to have emerged shortly before 300 thousand years ago (ka) in Africa, before dispersing to occupy all the world's biomes, from deserts to dense tropical rainforest[4,5]. Although grasslands and coasts have typically been given primacy in studies of the cultural and environmental context for human emergence and spread (for example, refs. 6–8), recent evidence has implicated several regions and ecosystems in the earliest prehistory of our species[3,9,10]. Rainforest habitation in Asia and Oceania is firmly documented as early as 45 ka (refs. 11,12), and perhaps as early as 73 ka (ref. 13). However, the oldest secure, close human associations with such wet tropical forests in Africa do not date beyond around 18 ka (refs. 6,14,15), despite evidence of the widespread presence of Middle Stone Age (MSA) assemblages in regions of present-day African rainforest[16,17] (Supplementary Information Section SI-1). Isotopic and zooarchaeological evidence from Panga ya Saidi in Kenya have supported an earlier use of mixed tropical forest and ecotonal environments from at least 77 ka (refs. 18,19), but clear evidence for the dedicated occupation of wet tropical forest remains lacking.

Here we report a suite of analyses from the site of Bété I, located in the Anyama locality of Côte d'Ivoire, West Africa (Fig. 1 and Extended Data Figs. 1–4), that demonstrates a deep-time association between humans and wet tropical forests dating to around 150 ka (Marine Isotope Stage (MIS) 6) (Fig. 2). This association is both geographically and ecologically distinct from contemporaneous sites known from across Africa. The site of Bété I (5.515° N, 4.06° W) is located approximately 20 km north of Abidjan, where an extensive Quaternary sequence is displayed in several deep sedimentary exposures revealed by quarrying activity (that is, Bété I–IV), as first reported in ref. 20. These were resolved into six stratigraphic units (F to A, from the base to the top) and further subdivided into 14 layers (Supplementary Information Section SI-1 and Supplementary Figs. 1–3) during excavations undertaken between 1982 and 1993 by a joint Ivorian–Russian mission that focused on an approximately 14-m step trench, with deeper exposures observed across the quarry site[21]. These broadly comprise a weathering horizon of the chloritic shale bedrock (Unit F), coarser alluvial deposits attributed to the Continental Terminal (Unit E), finer, gravel-free alluvial terre de barre deposits that show extensive weathering in the lower levels (Units D and C), along with recent subsoil (Unit B) and a topsoil horizon (Unit A). A radiothermoluminescence study initially dated the Unit E deposits to the Early and Middle Pleistocene. Although these ages should be regarded with extreme caution (see Supplementary Information Section SI-1 for a critical evaluation), an estimate of 254 ± 51 ka

[1]Centro Nacional de Investigación sobre la Evolución Humana (CENIEH), Burgos, Spain. [2]Human Palaeosystems Group, Max Planck Institute of Geoanthropology (MPI-GEA), Jena, Germany. [3]Histoire Naturelle des Humanités Préhistoriques (HNHP), CNRS–Université de Perpignan Via Domitia (UPVD)–Muséum national d'Histoire naturelle (MNHN), Paris, France. [4]Department of Archaeology, Classics, and Egyptology, University of Liverpool, Liverpool, UK. [5]Department of Life and Environmental Sciences, Bournemouth University, Poole, UK. [6]University of South Florida Libraries, University of South Florida, Tampa, FL, USA. [7]Départmente d'Histoire, Institut d'Histoire, d'Art et d'Archéologie Africains (IHAAA), Abidjan, Côte d'Ivoire. [8]School of Geography and Planning, University of Sheffield, Sheffield, UK. [9]Australian Research Centre for Human Evolution (ARCHE), Griffith University, Brisbane, Queensland, Australia. [10]Palaeoscience Labs, Department of Archaeology and History, La Trobe University Melbourne Campus, Bundoora, Victoria, Australia. [11]isoTROPIC Research Group, Max Planck Institute of Geoanthropology (MPI-GEA), Jena, Germany. [12]Department of Land Use and Urbanisation, Max Planck Institute of Geoanthropology (MPI-GEA), Jena, Germany. [13]Institute of Prehistoric Archaeology, University of Cologne, Cologne, Germany. [14]Department of Biological and Biomedical Sciences, School of Health and Behavioral Sciences, Bryant University, Smithfield, RI, USA. [15]Human Evolution Research Institute (HERI), Department of Geological Sciences, University of Cape Town, Cape Town, South Africa. [16]Université Cheikh Anta Diop de Dakar, Dakar, Senegal. [17]Institut des Sciences Anthropologiques de Développement (ISAD), Abidjan, Côte d'Ivoire. [18]Department of Anthropology, Loyola University Chicago, Chicago, IL, USA. [19]Department of Biology, Loyola University Chicago, Chicago, IL, USA. [20]Department of Classics and Archaeology, University of Malta, Msida, Malta. ✉e-mail: ben-arous@gea.mpg.de; j.blinkhorn@liverpool.ac.uk; scerri@gea.mpg.de

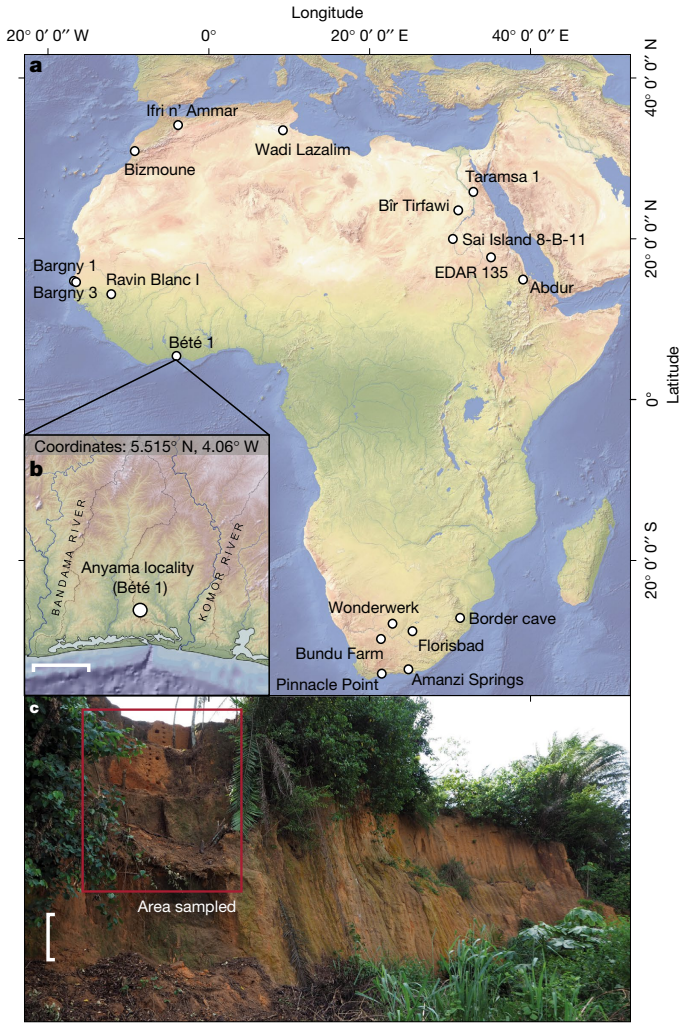

Fig. 1 | The Bété I site. a, General map showing the African sites dated to MIS 6 (around 130–190 ka). **b**, Location of Bété I site. **c**, Sequence at Bété I in 2020 after sampling for geochronology and palaeoecological proxies.

from Unit D in sediments underlying archaeological horizons provides a tentative terminus post quem for human presence at the site[21]. Dating of the nearby valley floor deposit has indicated an Early Holocene or terminal Pleistocene incision to establish the modern drainage, probably cutting the terrace deposits (Supplementary Information Section SI-2). Key stone tool assemblages recovered from Unit D include a prominent heavy tool component, such as picks (Supplementary Information Section SI-1 and Supplementary Figs. 1 and 4), alongside small retouched tools (Supplementary Information Section SI-1 and Supplementary Fig. 4). Unit C has assemblages with Levallois reduction and small retouched tools. Unfortunately, the lithic artefact collections were lost during the 2011 civil war.

Today, this site lies within the modern distribution of wet–humid West African tropical rainforest, which encompasses a diversity of forest types, including periodically to permanently inundated swamp and riparian forests, as well as evergreen rainforest[22,23]. Because the site represents the deepest stratified site yet found in Africa's (present-day) tropical forest regions, we returned to re-investigate it in 2020. The site was unfortunately destroyed later, between 2020 and 2021 (ref. 24), by quarrying activities.

We located the original step trench at Bété I, and cut back and cleaned the uppermost four steps of the original excavation, spanning the top 5.65 m of the sedimentary sequence. Our field records matched the sequence reported in ref. 21, comprising four discrete sedimentary units referred to as Units A–D. A suite of 37 sediment samples were recovered from this sequence for new sedimentological and palaeoecological analyses. The quantified description of the physical characteristics of the deposits matched those from the field records and previous studies, but also highlighted a discrete transition between Units C and D (Fig. 2, Supplementary Information Section SI-2 and Supplementary Fig. 5). The sedimentology supported the interpretation of a low-energy alluvial environment with episodic hiatuses presenting a high-resolution depositional setting for the archaeological assemblages (Supplementary Information Section SI-2 and Supplementary Table 1), with earlier identification of fine knapping debris at the site indicating little likelihood of post-depositional disturbance.

The chronology of the Bété I site was obtained using a combination of single-aliquot (SA) and single-grain (SG) optically stimulated luminescence (OSL) and multiple centre (MC) electron spin resonance (ESR) dating, both applied to quartz grains extracted from the sediments (Supplementary Information Section SI-3). In total, eight SA and SG-OSL and five MC-ESR ages (all reported with 1σ error) were calculated for various samples from Units C and D (Fig. 2 and Supplementary Information Section SI-3). The ages are, overall, stratigraphically consistent from the base to the top of the Bété I sequence, and range from the late Middle Pleistocene to the Pleistocene/Holocene transition, contributing to the establishment of a coherent age–depth model for the in situ stone tool assemblages from Units D and C. Our critical evaluation of the combined OSL-ESR dataset indicated that: (1) the SG-OSL results can be regarded as the most reliable estimates of the true burial age of the deposits; (2) the SG-OSL chronology is supported, in most samples, by the semi-independent age control provided by the SA-OSL and MC-ESR results; and (3) among the various sets of ESR ages obtained through the MC approach, those derived from the titanium centre of quartz (Ti–H) signal are regarded as providing a closer estimate to the true burial age. A complete discussion of the dating results is presented in Supplementary Information Section SI-3 (see also Supplementary Figs. 6–14 and Supplementary Tables 2–11) and Extended Data Figs. 5 and 6. At the bottom of the sequence, the SG-OSL age of the deepest sample, ANY20-09, was 166 ± 14 ka (placing it in MIS 6, 130–190 ka, ref. 25), providing a maximum age constraint for the deposits. The chronology of the lithic assemblages from Unit D, with the larger tool component, is bracketed by SG-OSL ages of 146 ± 9 ka (ANY20-08) and 55 ± 3 ka (ANY20-05). By comparison, the Ti–H ESR ages are older, but consistent at 1σ, because of their large associated uncertainties (Supplementary Information Section SI-3). In particular, sample ANY20-08 is associated with the deepest location of lithic artefacts in Unit D, and provides an age of around 150 ka (in MIS 6) for the earliest evidence of human presence at the site (Supplementary Information Section SI-3).

The ages of 35 ± 3 ka (SG-OSL) and 44 ± 19 ka (ESR) from the transition from Units D to C are relatively coherent, and agree at 1σ, indicating the end of Unit D deposition towards the end of MIS 3. Further up in the sequence, two SG-OSL ages from Unit C constrain the typical MSA artefacts to between 20 ± 1 ka (ANY20-03) and 12 ± 1 ka (ANY20-02), placing this unit in MIS 2.

The delta 13 carbon ($\delta^{13}C$) measurements of the bulk soil organic matter (SOM) from the sediments taken through the Bété I sequence are shown in Fig. 2, Supplementary Table 10 and Extended Data Fig. 7. The values range from −25.4 to −27.6‰ (−26.6 ± 0.6‰, n = 35) and overlap with the bulk $\delta^{13}C$ values measured from contemporary African rainforest contexts[26], corrected for the Suess effect[27–30], of −24.8 to −34.5‰ (−28.1 ± 1.9‰, n = 24). The SOM $\delta^{13}C$ is usually assumed to represent standing plant biomass and plant remains introduced by either humans (for example, carried for bedding or other uses) or nature (for example, from wind and water transport)[31], with an increase of +1 to +3 per mil in SOM $\delta^{13}C$ values relative to the contributing plant matter being the result of microbial activity[32]. With this in mind, the

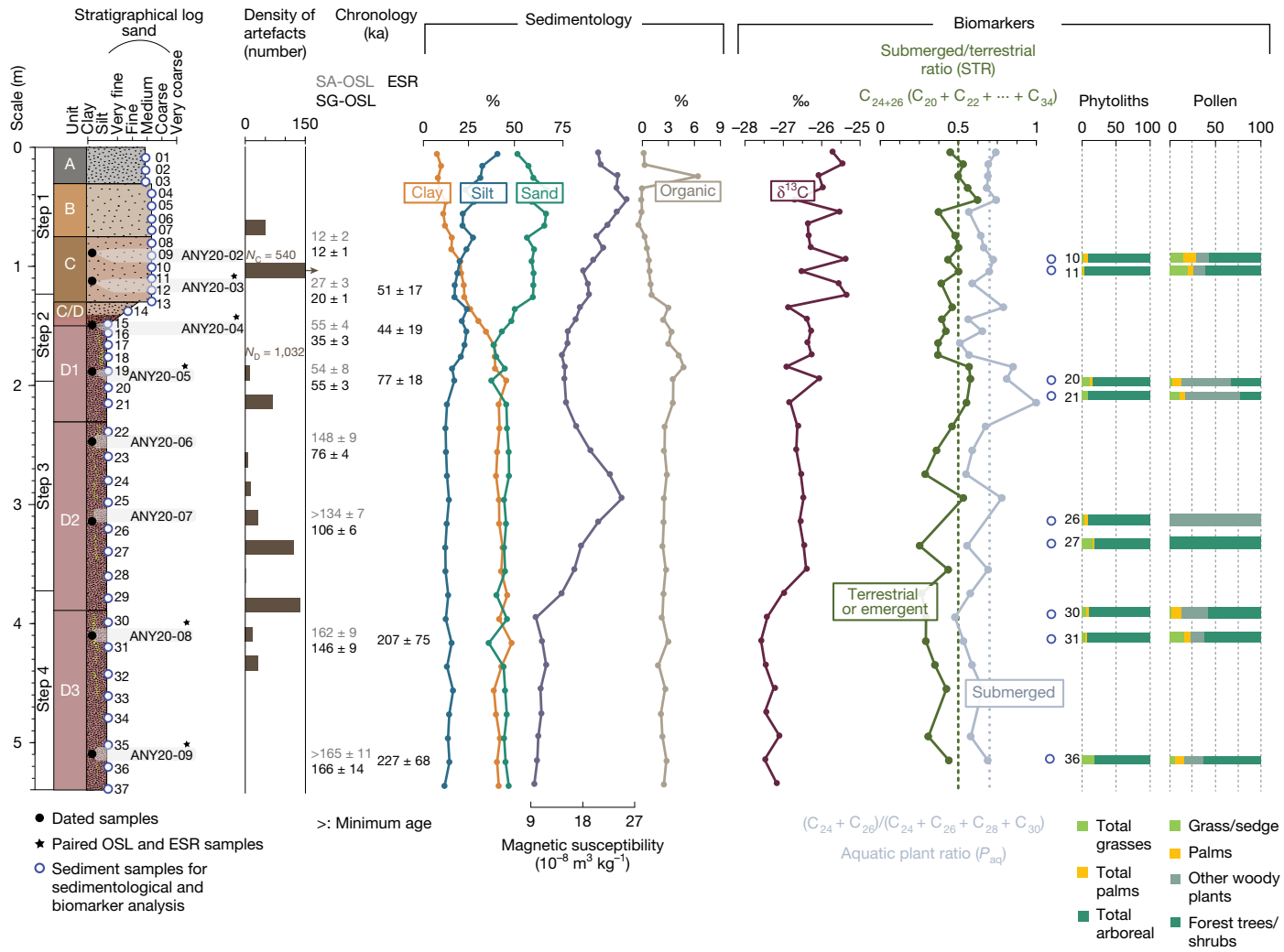

Fig. 2 | Stratigraphy, artefact density, geochronology, sedimentology and biomarkers from the Bété I sequence. Artefact densities are derived from ref. 21. Numerical age uncertainties are given at 1σ. NC and ND are the total numbers of lithics artefacts found in Units C and D, respectively.

Bété I bulk $\delta^{13}C$ values primarily indicate C3 biomass, with an increase in values recorded from sample 31 (Unit D3) to sample 29 (Unit D2), from 4.2 to 3.8 m deep, and $\delta^{13}C$ fluctuations from sample 21 (Unit D1, at 2.2 m deep) upwards with a steady trend towards increasing values towards the top of the sequence (Unit A). To discern the exact drivers of these trends, we combined this isotopic analysis with biomarker analyses (leaf-wax) and the examination of phytoliths and pollen from the sequence.

Of the 37 palaeoenvironmental samples, 31 had sufficient lipid material for plant wax biomarker analysis through gas chromatography mass spectrometry (GCMS). Even-numbered, mid-chain-length (C_{22}–C_{24}) *n*-alkanoic acids (as fatty acid methyl esters (FAMEs)) dominated the biomarker distributions, indicating high input from submerged or emergent plant wax sources for most samples[33,34]. The average chain length ($ACL_{20–34}$) ranged from 23.9 to 27.3 (25.2 ± 0.84, n = 31) (Supplementary Table 13), which is typically lower than previous reports of modern ACLs from African terrestrial plants[35–39]. The aquatic plant ratio (P_{aq} C_{22+24}) ranged from 0.41 to 0.86 (0.66 ± 0.09, n = 31), and the submerged/terrestrial ratio (STR) of the C_{24} FAME (STR_{24}) ranged from 0.15 to 0.44 (0.25 ± 0.07, n = 31) (Fig. 2 and Supplementary Table 13). Both proxies indicate that abundant wetland-adapted species, either fully submerged or emergent plants, were principal contributors of plant wax biomarkers to the site (Supplementary Information Section SI-4 and Supplementary Figs. 15 and 16). The STR values, however, indicate that terrestrial plants also provided plant wax biomarkers to the Bété I sediments. There also seems to be a changing pattern in the relationship between the abundance of the C_{24} FAME and the bulk sedimentary $\delta^{13}C$. For instance, below 2.0 m (from the lower section of Unit D3 to the middle of Unit D1), the $\delta^{13}C$ co-varies in the same direction as both the STR and P_{aq} (Spearman's correlation STR_{24} r_s = 0.248, P = 0.394; P_{aq} r_s = 0.597, P = 0.024). However, above 2.0 m (from the middle of Unit D1 to the middle of Unit A), there is an anti-phased correlation between the C_{24} FAME and the bulk sedimentary $\delta^{13}C$ (Spearman's correlation r_s = −0.377, P = 0.136). That is, as the abundance of C_{24} increases relative to the other FAMEs, the $\delta^{13}C$ decreases. Additionally, as both the STR and P_{aq} values increase, indicating greater input from submerged/aquatic plant biomarkers, the bulk sedimentary $\delta^{13}C$ shifts lower (Spearman's correlation STR_{24} r_s = −0.441, P = 0.077; P_{aq} r_s = −0.240, P = 0.353). It is possible that, as local forest characteristics changed, such as with forest succession, the bulk isotope signal changed in accordance with the abundance of terrestrial or aquatic plants.

Nine samples were analysed for phytoliths and pollen to establish the preservation and representation of microbotanical evidence, selected to match peak artefact densities, correlate to human habitation of the site, and provide further insights into the trends observed in the biochemical data. The deposition and preservation of these two types of plant microfossil is inversely correlated, such that samples with a

low phytolith influx (Supplementary Information Section SI-4 and Supplementary Fig. 17) tend to have a higher influx of pollen (Supplementary Information Section SI-4 and Supplementary Tables 15 and 16), but every sample yielded plant microfossils.

The phytolith assemblages produced by nine samples (samples 10, 11, 21, 22, 26, 27, 30, 31 and 36) (Supplementary Table 14) established their preservation. Morphotype identification demonstrated that all samples were dominated by arboreal phytolith morphotypes (Extended Data Fig. 8), with 82–96% of these morphotypes representing trees/shrubs, and therefore being indicative of a C3-dominated biomass in all cases (Supplementary Fig. 18). All of the arboreal phytolith types identified in the nine sediment samples are produced in most dicotyledons, so they could not be attributed to the genus or species level. Arecaceae phytoliths (palms) made up between 2 and 7% of the identified assemblages in seven of the nine samples, reaching a maximum in the uppermost sample (sample 10). Grass phytoliths made up between 1 and 18% of the assemblage, with the highest values coming from the lowermost sample (sample 36). Grasses peak again in sample 27 (16%) and fell to their lowest percentages in the uppermost unit (sample 10, 3%, and sample 11, 1%). It was not possible to directly compare the number of phytoliths produced by monocots and dicots because plants have different abilities to produce phytoliths—in particular, the Poaceae produce more than other monocotyledons[40]. As monocotyledons can produce up to 20 times more phytoliths than the dicots[41], the dominance of arboreal phytoliths in all samples (more than 81%) is a clear signal of local forest cover with relatively few grasses or palms.

The pollen assemblages (Supplementary Figs. 19–26, Supplementary Tables 16 and 17 and Extended Data Fig. 9) in these samples were dominated by dicot pollen types (70–80%), followed by grasses (10–20%) and palms (5–10%). The pollen types were attributable to species, in some cases (*Elaeis guineensis* Jacq.), and to the genus (*Hunteria*) or family (Poaceae) level in others. There was a consistent presence of pollen types typical of wet–humid West African rainforests, riparian forests and swamp forests. Early riparian forest succession is signalled by the co-occurrence of *E. guineensis* (oil palm), dense shrubs/trees belonging to the genera *Alchornea* and *Macaranga*, and gap-colonizing trees, such as *Anthocleista* (Supplementary Fig. 22 and Supplementary Table 17). *Canarium schweinfurthii* and *Pentadesma* are both large trees frequently found in the later stages of forest succession in seasonally inundated conditions near rivers and lakes. These pollen types were more common in Unit D (specifically in the middle of D2 and the top of D3) and were absent from Unit C, being replaced by *Uapaca*, which is a diverse genus with many riparian-affiliated species. Unit C also yielded taxa typical of riparian forests (*Parinari* sp.), as well as types widespread in the Guineo–Congolian forest zone (*Rauvolfia* sp.). The Unit D samples contained more *Hunteria* pollen, probably attributable to *Hunteria umbellata*, which is common in wet–moist West African tropical rainforests[23], particularly in forests adjacent to waterways[42]. The presence of anther fragments from *E. guineensis* and *Hunteria* (Fig. 3) in sample 30 from the top of Unit D3 presents strong evidence for whole flowers/anthers falling directly from the plant and being incorporated into the sedimentary matrix, supporting the local rainforest signal.

The SG-OSL dates of around 20–12 ka for the MSA assemblage in Unit C and 150–55 ka for the assemblages differentiated by a large tool component in Unit D document persistent human occupation of the Anyama area after the Middle Pleistocene. However, it is the lithic assemblages in Unit D that are of particular interest, as they are associated with a wet and forested environment. The palaeoenvironmental proxies from Unit D show no evidence for open and dry grassland, sparse savannah, or wooded savanna vegetation cover, despite the tendency for grasses to be over-represented in microfossil records. The sedimentary, biomarker and microfossil results are remarkably consistent, showing evidence for alluvial deposition in a tropical forest environment and consisting of riparian, swamp and rainforest taxa. Currently, the assemblages of Bété I from Unit D dating from MIS 6 are the oldest found outside the sahelian and sudanian savannah biomes of West Africa (Fig. 4). On a broader scale, the Unit D lithic assemblages are contemporaneous with other MIS 6 MSA stone tool assemblages found in other African sites located in different ecoregions, such as savannahs, or close to modern coasts ($n = 16$) (Fig. 1 and Supplementary Table 18 in Supplementary Information Section SI-5 and references therein) in West Africa (Bargny 1 and Bargny 3), in northern Africa (Bizmoune, Ifri n'Ammar, Wadi Lazalim (site 16/29), Bîr Tirfawi, Taramsa 1), in eastern Africa (Sai Island 8-B-11, EDAR 135, Abdur) and in South Africa (Amanzi Springs, Florisbad, Pinnacle Point 13B, Wonderwerk, Border Cave, Bundu Farm).

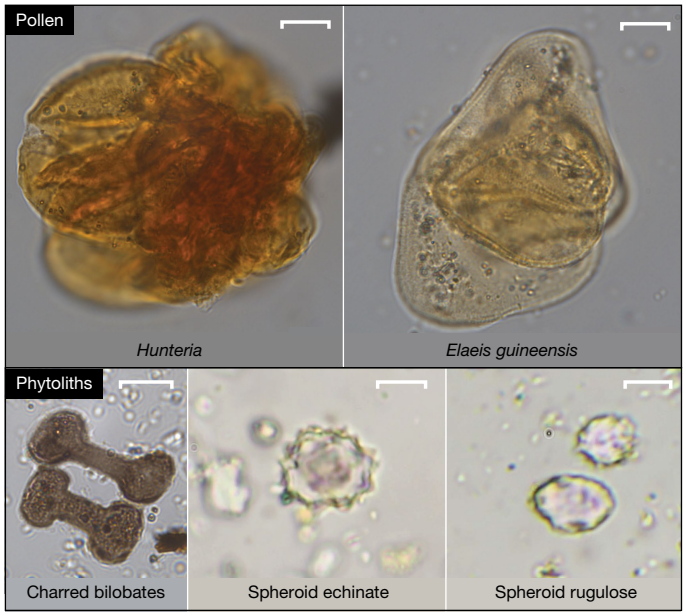

Fig. 3 | Key pollen and phytolith taxa found at Bété I. Examples of anther fragments (sample 30) from pollen taxa typical of rainforest (*Hunteria*) and flooded forest (*E. guineensis*) and phytoliths (respectively from samples 20, 30 and 22) preserved in Unit D of the Bété I sequence. Scale bar, 10 µm.

Several independent lines of evidence have confirmed the association between humans and tropical wet broadleaf forest at Anyama, starting at least 150 ka. The consistent forest signal over time also indicates that this area of West Africa possibly acted as a rainforest refugium during arid periods (Supplementary Information Section SI-4). This corroborates projections of Middle and Late Pleistocene vegetation showing reduced, but persistent, rainforest cover at lower latitudes[43]. These data confirm a deep-time connection between human evolution and wet tropical forests, and highlight the importance of Africa's many biomes and diverse ecoregions in this process[9,44]. The assemblages from Unit C, featuring Levallois flakes and points, side and end retouched pieces, add to the emerging evidence of a chronologically persistent MSA in West Africa towards the end of the Late Pleistocene that is probably a key regional characteristic[7,45].

The assemblage in Unit D, featuring large tools alongside a small tool component, may support long-held views that the diverse heavy-duty tool assemblages seen in Central and West Africa are convergent adaptive solutions to tropical forest habitation[6,16]. The combination of an MIS 6 age with the ecological context of the Unit D assemblage is without precedent elsewhere in Africa. As a result, the archaeological classification of the Unit D assemblage warrants circumspection and further study (Supplementary Information Section SI-1). This is particularly the case because West Africa remains under-researched compared

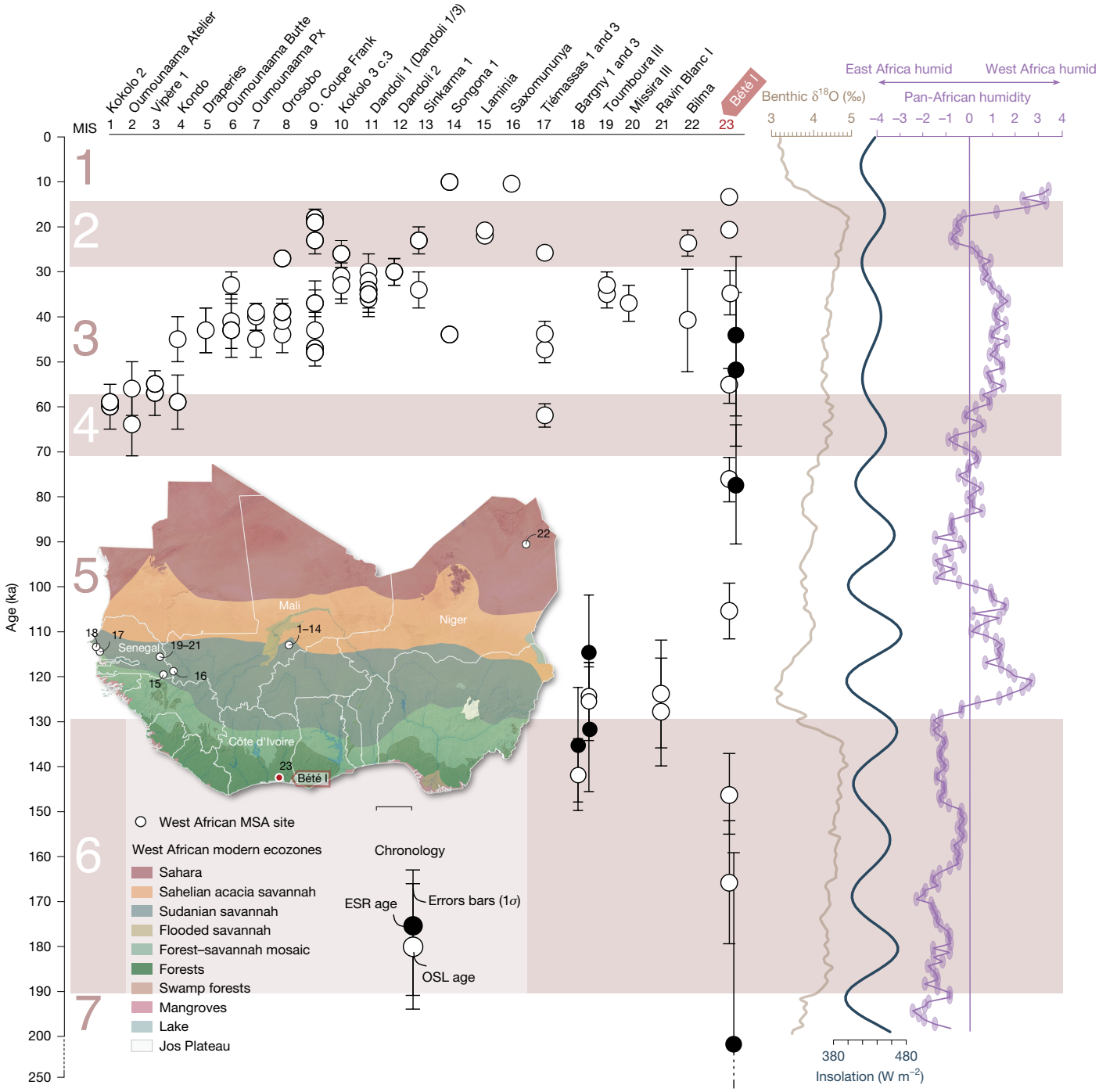

Fig. 4 | West African dated Stone Age sites with key off-site palaeoenvironmental proxy records. Insolation curve (dark blue) from ref. 46. Inter-regional African humidity curve (purple) from ref. 47. Benthic curve (light brown) built from ref. 48. Synthesis of dated occupations from West Africa from refs. 48–50 (for more details, see Supplementary Information Section SI-5). The Later Stone Age sites are not included. Error bars associated with OSL and ESR ages represent ±1σ uncertainties.

to other regions of the continent, and its archaeological sequence and specific regional characteristics are yet to be fully understood (Fig. 2 and Supplementary Information Section SI-1). Most importantly, however, our results confirm a deep-time connection between human evolution and tropical forest biomes, opening up a new chapter in the human past in which our species occupied dense, wet tropical forests much earlier than widely thought. This association confirms the predictions of the pan-African model of human evolution, and highlights the importance of Africa's many regions and ecosystems in this process[9].

Online content

Any methods, additional references, Nature Portfolio reporting summaries, source data, extended data, supplementary information, acknowledgements, peer review information; details of author contributions and competing interests; and statements of data and code availability are available at https://doi.org/10.1038/s41586-025-08613-y.

1. Hublin, J.-J. et al. New fossils from Jebel Irhoud, Morocco and the pan-African origin of *Homo sapiens*. *Nature* **546**, 289–292 (2017).

2. Richter, D. et al. The age of the hominin fossils from Jebel Irhoud, Morocco, and the origins of the Middle Stone Age. *Nature* **546**, 293–296 (2017).
3. Scerri, E. M. L., Chikhi, L. & Thomas, M. G. Beyond multiregional and simple out-of-Africa models of human evolution. *Nat. Ecol. Evol.* **3**, 1370–1372 (2019).
4. Roberts, P. & Stewart, B. A. Defining the 'generalist specialist' niche for Pleistocene *Homo sapiens*. *Nat. Hum. Behav.* **2**, 542–550 (2018).
5. Groucutt, H. S. et al. Multiple hominin dispersals into Southwest Asia over the past 400,000 years. *Nature* **597**, 376–380 (2021).
6. Mercader, J. Forest people: the role of African rainforests in human evolution and dispersal. *Evol. Anthropol. Issues News Rev.* **11**, 117–124 (2002).
7. Scerri, E. M. L. et al. Continuity of the Middle Stone Age into the Holocene. *Sci. Rep.* **11**, 70 (2021).
8. Ben Arous, E. et al. An improved chronology for the Middle Stone Age at El Mnasra cave, Morocco. *PLoS ONE* **17**, 1–28 (2022).
9. Scerri, E. M. L. et al. Did our species evolve in subdivided populations across Africa, and why does it matter? *Trends Ecol. Evol.* **33**, 582–594 (2018).
10. Ragsdale, A. P. et al. A weakly structured stem for human origins in Africa. *Nature* **617**, 755–763 (2023).
11. Barker, G. et al. The 'human revolution' in lowland tropical Southeast Asia: the antiquity and behavior of anatomically modern humans at Niah Cave (Sarawak, Borneo). *J. Hum. Evol.* **52**, 243–261 (2007).
12. Summerhayes, G. R. et al. Human adaptation and plant use in Highland New Guinea 49,000 to 44,000 years ago. *Science* **330**, 78–81 (2010).
13. Westaway, K. E. et al. An early modern human presence in Sumatra 73,000–63,000 years ago. *Nature* **548**, 322–325 (2017).
14. Mercader, J. & Brooks, A. S. Across the forests and savannas: Later Stone Age assemblages from Ituri and Semliki, Democratic Republic of Congo. *J. Anthropol. Res.* **57**, 197–217 (2001).
15. Roberts, P. *Tropical Forests in Prehistory, History, and Modernity* (Oxford Academic, 2019).
16. Taylor, N. in *Africa from MIS 6-2: Population Dynamics and Paleoenvironments* (eds Jones, S. C. & Stewart, B. A.) 273–299 (Springer, 2016).
17. Padilla-Iglesias, C., Grove, M. & Blinkhorn, J. Ecological drivers of hunter-gatherer lithic technology from the Middle and Later Stone Age in Central Africa. *Quat. Sci. Rev.* **322**, 108390 (2023).
18. Shipton, C. et al. 78,000-year-old record of Middle and Later Stone Age innovation in an East African tropical forest. *Nat. Commun.* **9**, 1832 (2018).
19. Roberts, P. et al. From forests to the coast – multidisciplinary investigation of human adaptations at the Mini-athiliya shell midden, Sri Lanka. *Anc. Lanka* https://doi.org/10.29173/anlk650 (2022).
20. Chenorkian, R. & Paradis, G. Une industrie paléolithique découverte dans la «terre de barre» d'une terrasse proche d'Anyama (région d'Abidjan). *Nyame Akuma* **21**, 18–27 (1982).
21. Lioubin, V. P. & Guédé, F. Y. The Palaeolithic of the Republic of Cote d'Ivoire (West Africa) [in Russian]. In *Proceedings of the Institute of the History of Material Culture* Vol. 3 (Russian Academy of Sciences, 2000).
22. White, F. The vegetation of Africa: a descriptive memoir to accompany the UNESCO/AETFAT/UNSO vegetation map of Africa. *Geogr. J.* **151**, 108 (1983).
23. Fayolle, A. et al. Patterns of tree species composition across tropical African forests. *J. Biogeogr.* **41**, 2320–2331 (2014).
24. Dibié, C. N. & Yiodé, F. G. Recherches prehistoriques en Côte d'Ivoire: non-développements récents sur le site d'Anyama (district d'Abidjan). *L'Anthropologie* **127**, 103215 (2023).
25. Lisiecki, L. E. & Raymo, M. E. A Pliocene–Pleistocene stack of 57 globally distributed benthic delta^{18}O records. *Paleoceanography* **20**, 1–17 (2005).
26. Vogts, A., Moossen, H., Rommerskirchen, F. & Rullkötter, J. Distribution patterns and stable carbon isotopic composition of alkanes and alkan-1-ols from plant waxes of African rain forest and savanna C3 species. *Org. Geochem.* **40**, 1037–1054 (2009).
27. Verburg, P. The need to correct for the Suess effect in the application of $\delta^{13}C$ in sediment of autotrophic Lake Tanganyika, as a productivity proxy in the Anthropocene. *J. Paleolimnol.* **37**, 591–602 (2007).
28. Hare, V. J., Loftus, E., Jeffrey, A. & Ramsey, C. B. Atmospheric CO_2 effect on stable carbon isotope composition of terrestrial fossil archives. *Nat. Commun.* **9**, 1–8 (2018).
29. Francey, R. J. et al. A 1000-year high precision record of $\delta^{13}C$ in atmospheric CO_2. *Tellus B: Chem. Phys. Meteorol.* **51**, 170 (1999).
30. Keeling, C. D. et al. *Exchanges of Atmospheric CO_2 and $^{13}CO_2$ with the Terrestrial Biosphere and Oceans from 1978 to 2000. I. Global Aspects*. Ref. No. 01-06 (Scripps Institute of Oceanography, 2001).
31. Ambrose, S. H. & Sikes, N. E. Soil carbon isotope evidence for Holocene habitat change in the Kenya Rift Valley. *Science* **253**, 1402–1405 (1991).
32. Ehleringer, J. R., Buchmann, N. & Flanagan, L. B. Carbon isotope ratios in belowground carbon cycle processes. *Ecol. Appl.* **10**, 412 (2000).
33. Ficken, K. J., Li, B., Swain, D. L. & Eglinton, G. An n-alkane proxy for the sedimentary input of submerged/floating freshwater aquatic macrophytes. *Org. Geochem.* **31**, 745–749 (2000).
34. Liu, H. & Liu, W. Concentration and distributions of fatty acids in algae, submerged plants and terrestrial plants from the northeastern Tibetan Plateau. *Org. Geochem.* **113**, 17–26 (2017).
35. Bush, R. T. & McInerney, F. A. Leaf wax n-alkane distributions in and across modern plants: implications for paleoecology and chemotaxonomy. *Geochim. Cosmochim. Acta* **117**, 161–179 (2013).
36. Carr, A. S. et al. Leaf wax n-alkane distributions in arid zone South African flora: environmental controls, chemotaxonomy and palaeoecological implications. *Org. Geochem.* **67**, 72–84 (2014).
37. Dodd, R. S. & Poveda, M. M. Environmental gradients and population divergence contribute to variation in cuticular wax composition in *Juniperus communis*. *Biochem. Syst. Ecol.* **11**, 1257–1270 (2003).
38. Duan, Y. & Xu, L. Distributions of n-alkanes and their hydrogen isotopic composition in plants from Lake Qinghai (China) and the surrounding area. *Appl. Geochem.* **27**, 806–814 (2012).
39. Rommerskirchen, F., Plader, A., Eglinton, G., Chikaraishi, Y. & Rullkötter, J. Chemotaxonomic significance of distribution and stable carbon isotopic composition of long-chain alkanes and alkan-1-ols in C4 grass waxes. *Org. Geochem.* **37**, 1303–1332 (2006).
40. Zuo, X. X. & Lü, H. Y. Carbon sequestration within millet phytoliths from dry-farming of crops in China. *Chinese Sci. Bull.* **56**, 3451–3456 (2011).
41. Albert, R. & Weiner, S. in *Phytoliths, Applications in Earth Sciences and Human History* Vol. I (eds Meunier, J. D. & Coline, F.) Ch. 19 (Balkema, 2001).
42. Owusu, G., Anning, A. K., Belford, E. J. D. & Acquah, E. Plant species diversity, abundance and conservation status of the Ankasa Resource Reserve, Ghana. *Trees For. People* **8**, 100264 (2022).
43. Dupont, L. M., Jahns, S., Marret, F. & Ning, S. Vegetation change in equatorial West Africa: time-slices for the last 150 ka. *Palaeogeogr. Palaeoclimatol. Palaeoecol.* **155**, 95–122 (2000).
44. Patalano, R. et al. Microhabitat variability in human evolution. *Front. Earth Sci.* **9**, 1–19 (2021).
45. Chevrier, B. et al. Between continuity and discontinuity: an overview of the West African Paleolithic over the last 200,000 years. *Quat. Int.* **466**, 3–22 (2018).
46. Laskar, J. et al. A long-term numerical solution for the insolation quantities of the Earth. *Astron. Astrophys.* **428**, 261–285 (2004).
47. Kaboth-Bahr, S. et al. Paleo-ENSO influence on African environments and early modern humans. *Proc. Natl Acad. Sci. USA* **118**, e2018277118 (2021).
48. Douze, K. et al. A West African Middle Stone Age site dated to the beginning of MIS 5: archaeology, chronology, and paleoenvironment of the Ravin Blanc I (eastern Senegal). *J. Hum. Evol.* **154**, 102952 (2021).
49. Niang, K., Blinkhorn, J., Bateman, M. D. & Kiahtipes, C. A. Longstanding behavioural stability in West Africa extends to the Middle Pleistocene at Bargny, coastal Senegal. *Nat. Ecol. Evol.* **7**, 1141–1151 (2023).
50. Ben Arous, E. et al. Constraining the age of the Middle Stone Age locality of Bargny (Senegal) through a combined OSL-ESR dating approach. *Quat. Environ. Humans* **2**, 100044 (2024).

Methods

Geochronology

Owing to the absence of organic/bone remains or minerals from volcanic deposits, the use of dating methods such as uranium (U) series, ESR combined with uranium-series, or argon/argon was not possible. The chronology of the Bété I site was therefore constrained using a combination of OSL and ESR dating methods, both applied to optically bleached quartz grains through a range of techniques and measurement procedures (single/multiple aliquots (SA/MA), single/multiple grains (SG/MG), multiple centre (MC) approach). Eight samples were dated along the sequence using SA-OSL and SG-OSL, whereas three replicate ESR ages (aluminium (Al), Ti–H and Ti–mix signals) were calculated for five of these samples.

Luminescence dating and palaeodose evaluation. Eight sediment samples (Supplementary Table 2) from the Bété I excavated sequence were collected using opaque metal tubes (25 cm in length and 4 cm in diameter). Three sediments were sampled from Unit C, one at the interface between Units C and D and five from Unit D. The samples were taken from sections extended following the first excavations of the site. The samples cover the uppermost 5 m of the stratigraphic sequence. Sample preparation was carried out at the Sheffield Luminescence Dating Laboratory (University of Sheffield, UK) (for the detailed preparation procedure and analysis of the samples, see Supplementary Information Section SI-3). The OSL measurements were undertaken both at the small aliquot (2 mm diameter; SA) and SG levels. The OSL dose reconstruction using the SA regenerative-dose (SAR) protocol[51] involved a single saturating exponential fit for younger samples and an exponential and linear fit for older samples. Samples were accepted for further analysis based on the following criteria: (1) the OSL signal measured 3σ above background; (2) the SAR growth curve passed within 1σ errors of the regenerative dose points; (3) the recycling values were within ±10% of unity for SA and ±20% for SG; and (4) the error on the test dose used in the SAR protocol was less than 10% for SA and 20% for SG. Equivalent doses (D_e) were determined using the central age model[52], minimum age model[52] and finite-mixture model[53,54]. The final selected D_e for each sample was divided by the dose rate (Supplementary Information Section SI-3 and the 'Dose rate evaluation' section) to derive the burial ages.

ESR dating and dose evaluation. One sediment sample from Unit C (ANY20-03), one from the interface between Units C and D1 (ANY20-04) and three from Units D1 and D3 (ANY20-09, ANY20-08 and ANY20-05) delivered sufficient quartz material for ESR dating. The MC approach[55] was employed, while the standard multiple aliquot additive dose method was used for the dose determination. Each quartz sample was divided into 14 aliquots—one natural (non-irradiated), one ultraviolet-bleached and 12 laboratory gamma-irradiated aliquots, irradiated up to about 23 kGy. The Al and Ti signals were repeatedly measured in each sample, three to four times over different days, and were corrected by their corresponding receiver gain value, temperature factor[56], number of scans and aliquot mass. The noise was extracted and subtracted from the Ti ESR intensities following ref. 57. Dose response curves for each signal were obtained from the mean ESR intensity values and associated 1 s.d. derived from the repeated measurements. The experimental points were fitted using Microcal OriginPro (OriginLab Corporation) using a Levenberg–Marquardt algorithm by chi-square minimization, and several fitting functions were tested for D_e determination (Supplementary Information Section SI-3). The final D_e uncertainties included a dose rate calibration error (1σ) of 2.3%. The detailed analytical procedure can be found in Supplementary Information Section SI-3.

Dose rate evaluation. For the ESR and OSL dating analyses, the total dose rate was derived from laboratory measurements. For each dated sample, approximately 3–5 g of dry milled sediment were analysed by inductively coupled plasma mass spectrometry to quantify the potassium (K), thorium (Th), U and rubidium (Rb) concentrations. These concentration values were used to calculate the alpha, beta and gamma dose rate components using conversion factors from ref. 58. In addition, approximately 30 g of this same raw sediment, previously dried and powdered, were analysed by high-resolution gamma spectrometry using a high-purity germanium detector to identify possible disequilibrium in the U^{238} decay chain. Dose rate values were calculated for a grain-size fraction of 180–212 μm (nominal sieve opening sizes) and an assumed thickness removed by hydrofluoric acid etching of 10 ± 5 μm (ref. 59). The values were corrected using beta and alpha attenuation values for spherical grains[60,61]. An internal dose rate of 30 ± 10 μGy per annum was considered, as commonly used in OSL and ESR dating application studies[62]. An alpha efficiency of 0.07 ± 0.01 (ref. 63) was used. The ESR and OSL dose rates and ages were calculated using the dose-rate and age calculator from ref. 64 (v.1.2) and the errors were 1σ. For both datasets, we used the same cosmic dose-rate values using the formula from ref. 65, with depth, altitude and latitude corrections applied[66]. Palaeomoisture contents were applied based on estimations of the average long-term burial water contents, with an associated absolute uncertainty of ±5% (see Supplementary Information Section SI-3.4 for further details).

Sedimentology and palaeoecology

Thirty-seven sediment samples were collected from along the sedimentary sequence (Fig. 2) for sedimentology, stable isotope, plant wax biomarker, phytolith and pollen analyses.

Sedimentology. For laser particle-size analysis, sieved sediment samples (approximately 1 g, less than 2 mm) were bathed in sodium hexametaphosphate solution (0.5%) for 24 h and then agitated in an ultrasonic bath, with the samples rinsed in purified water before analysis in a Malvern Mastersizer 3000. Characterization of the grain-size results was conducted using GRADISTAT software[67]. For loss-on-ignition analysis, sediment samples (approximately 10 g) were weighed (to three decimal places—0.001 g) and heated in a muffle furnace to 105 °C, 550 °C and 950 °C (allowing the samples to cool to 105 °C for weighing between steps) to calculate the proportions of water, total organic matter, carbonates and mineral residue. Magnetic susceptibility was measured in the laboratory using a Bartington MS3 magnetic susceptibility meter coupled with an MS3B sensor to analyse approximately 12-g samples, weighed on precision scales, to allow calculation of the mass specific values, presented as X_{mass} (10^{-8} m^3 kg^{-1}).

Stable isotope. The preparation of the bulk organic matter stable isotope samples, and their associated analysis, was as follows. Bulk sediment samples were weighed and sieved through a 2-mm mesh to remove stones and large macrobotanical materials. Then, 2 M hydrochloric acid (HCl) was added to 1 g of each sieved sample to remove any carbonates before the samples were rinsed three times using deionized water, interspersed with centrifugation. The remaining residues were then freeze-dried for 48 h. Duplicates of 1-mg aliquots of dry sample were weighed out into tin capsules. The $\delta^{13}C$ measurements of the samples were measured using a Thermo Scientific Flash 2000 elemental analyser coupled with a Thermo Delta V Advantage mass spectrometer at the Isotope Laboratory, MPI-GEA, Jena. The isotopic values are reported as the ratio of the heavier isotope to the lighter isotope ($^{13}C/^{12}C$) as δ values in parts per mil relative to the Vienna Pee Dee Belemnite (VPDB) standard. The results were calibrated against international standards—IAEA-CH-6 ($\delta^{13}C = -10.49 \pm 0.47‰$) and USGS40 ($\delta^{13}C = 26.38 \pm 0.042‰$). The international standard USGS61 ($\delta^{13}C = -35.05‰$) was used to check machine precision. On the basis of replicate analyses, the long-term machine error over a year was ±0.2‰ for $\delta^{13}C$. The overall measurement precision was recorded throughout.

Plant wax biomarker analysis. Dry, homogenized sediments (approximately 20 g) were extracted using a Büchi SpeedExtractor E-916 pressurized speed extractor and 9:1 (v/v) dichloromethane to methanol at 100 °C and 103 bar (1,500 psi) in three, 10-min cycles. The total lipid extract (TLE) was separated into neutral, acid and polar fractions by aminopropyl column chromatography. The acid fraction was methylated to produce FAMEs and isolated using silica gel column chromatography. The FAMEs were then analysed using an Agilent 7890B gas chromatography (GC) system equipped with an Agilent HP-5 capillary column (30 m long, 0.25 mm internal diameter and a 0.25-µm film) coupled to a 5977 A Series mass selective detector (MSD) at the Max Planck Institute of Geoanthropology (Jena, Germany). The FAMEs were identified by comparing their mass spectra and retention times against an external standard mixture. See Supplementary Information Section SI-4 for further details on the biomarker molecular characterizations.

Phytoliths. The phytolith samples were processed using a standard phytolith extraction protocol as follows: (1) the sample was screened through a 0.5-mm mesh to remove coarse-sized particles; (2) approximately 2 g of dried raw sediment was weighed out; (3) the calcium carbonates were dissolved using a dilution of 10% HCl, the samples then being washed in distilled water three times; (4) the clay was removed using a settling procedure and sodium hexametaphosphate (Calgon) as a dispersant. Distilled water was added and the samples were left for 75 min before the suspension was poured off. This was repeated at hourly intervals until the samples were clear. The samples were then transferred into crucibles and left to dry at a temperature of less than 50 °C; (5) after drying, the samples were placed in a muffle furnace for 2 h at 500 °C to remove the organic matter; (6) the phytoliths were then separated from the remaining material using a heavy liquid calibrated to a specific gravity of 2.3. The phytoliths were transferred to centrifuge tubes and washed three times in distilled water. They were then placed in small Pyrex beakers and left to dry; (7) approximately 2 mg of phytoliths per sample were mounted onto microscope slides, using the mounting medium Entellan. The microscope slides were assessed using a Meiji MT4300L transmitted light microscope using ×100 and ×400 magnifications. The phytoliths were counted and categorized into types, and further classified as deriving from either woody (dicotyledon) or non-woody (monocotyledon) taxa.

The weight percentage of the phytoliths produced by each sediment sample was calculated by dividing the weight of the phytoliths extracted from the sample by the original sample weight multiplied by 100 (Supplementary Fig. 11). This number is an approximation because other siliceous materials may also have been extracted at the same time (for example, diatoms and sponge spicules), and some residual material is likely to remain in the extracted samples.

Pollen. The samples for pollen analysis (Supplementary Table 11) were shipped to the IASCE Paleoecology Laboratory at the University of South Florida, Tampa. The samples were weighed and their volumes were estimated using displacement. Two tablets of *Lycopodium* sp. spores were added to each sample (batch no. 100320201) and dissolved with 10% HCl. The samples were centrifuged–decanted–rinsed until pH neutral, and then placed on a shaker overnight in Calgon solution (10% sodium hexametaphosphate). The fine materials were isolated using gravity separation and screening through 250-µm sieves. Degraded and other complex organics were digested in a 10-min hot bath at 80 °C in a 10% potassium hydroxide solution. The samples were then centrifuged, the solution decanted, and a small (approximately 0.5 ml) volume of concentrated (27%) HCl was added to the samples. The samples were centrifuged–decanted–rinsed again until their pH became neutral and the supernatant was clean. The samples were rinsed in 99% glacial acetic acid, centrifuged and decanted, and then were treated using the acetolysis reaction series. Acetolysis was triggered by the addition of a 9:1 solution of acetic anhydride and sulfuric acid, each at stock concentrations (99.5% and 48%, respectively). The samples were left in a 90 °C hot bath for 6 min, centrifuged and decanted, rinsed in glacial acetic acid, and then centrifuged–decanted–rinsed until pH neutral. Microbotanical fossils were recovered from the remaining residue using density separation in a solution of 5% HCl and zinc bromide at a specific gravity of 2.3 g ml^{-1}. At this density, we were able to retrieve both pollen and phytoliths from the samples. This material was retrieved from density separation in ethanol using a pipette, and then transferred into glycerin and stored in dram vials.

The samples were mounted onto glass slides in glycerin and were fixed under a coverslip using fingernail polish. Analysis was conducted using a binocular light microscope to count the number of *Lycopodium* tracer spores, native fern spores and pollen encountered during vertical transects across the microscope slide at ×400 magnification. The pollen and spores were photographed and identified at ×400 and ×1,000 magnification using published reference material[68–70], online reference material (African Pollen Database) and unpublished digitized reference material collected from Göthe Universität (Frankfurt, Germany), the Muséum national d'Histoire naturelle (MNHN, Paris, France) and Centre de Recherche et d'Enseignement en Géosciences de l'Environnement (CEREGE Arbois, Aix-en-Provence, France). The tracers, spores and pollen were tallied until either a total of 200 pollen grains or 100 *Lycopodium* spores were encountered.

Reporting summary

Further information on research design is available in the Nature Portfolio Reporting Summary linked to this article.

Data availability

All relevant data are provided with the paper and its Supplementary Information. Figures were created using Adobe Illustrator v.25.2.3, ArcMap v.10.5 and GIMP v.2.10.38.

51. Murray, A. S. & Wintle, A. G. Luminescence dating of quartz using an improved single-aliquot regenerative-dose protocol. *Radiat. Meas.* **32**, 57–73 (2000).
52. Galbraith, R. F., Roberts, R. G., Laslett, G. M., Yoshida, H. & Olley, J. M. Optical dating of single and multiple grains of quartz from Jinmuim rockshelter, northern Australia: Part I, experimental design and statistical models. *Archaeometry* **41**, 339–364 (1999).
53. Galbraith, R. F. & Green, P. F. Estimating the component ages in a finite mixture. *Int. J. Radiat. Appl. Instrumentation. Part D. Nucl. Tracks Radiat. Meas.* **17**, 197–206 (1990).
54. Roberts, R. G., Galbraith, R. F., Yoshida, H., Laslett, G. M. & Olley, J. M. Distinguishing dose populations in sediment mixtures: a test of single-grain optical dating procedures using mixtures of laboratory-dosed quartz. *Radiat. Meas.* **32**, 459–465 (2000).
55. Toyoda, S., Voinchet, P., Falgueres, C., Dolo, J.-M. & Laurent, M. Bleaching of ESR signals by the sunlight: a laboratory experiment for establishing the ESR dating of sediments. *Appl. Radiat. Isot.* **52**, 1357–1362 (2000).
56. Duval, M. & Guilarte Moreno, V. Assessing the influence of the cavity temperature on the ESR signal of the aluminum center in quartz grains extracted from sediment. *Anc. TL* **30**, 11–16 (2012).
57. Ben Arous, E., Duval, M. & Bateman, M. D. ESR dating of optically bleached quartz grains from Plio-Pleistocene to Holocene coastal dune deposits (Wilderness–Knysna area, South Africa): a comparison with luminescence. *Quat. Geochronol.* **70**, 101293 (2022).
58. Guérin, G., Mercier, N. & Adamiec, G. Dose-rate conversion factor: update. *Anc. TL* **29**, 5–8 (2011).
59. Duval, M. et al. Quantifying hydrofluoric acid etching of quartz and feldspar coarse grains based on weight loss estimates: implication for ESR and luminescence dating studies. *Anc. TL* **36**, 1–14 (2018).
60. Brennan, B. J. Beta doses to spherical grains. *Radiat. Meas.* **37**, 299–303 (2003).
61. Brennan, B. J., Lyons, R. G. & Phillips, S. W. Attenuation of alpha particle track dose for spherical grains. *Int. J. Radiat. Appl. Instrumentation. Part D. Nucl. Tracks Radiat. Meas.* **18**, 249–253 (1991).
62. Duval, M. et al. Re-examining the earliest evidence of human presence in Western Europe: new dating results from Pirro Nord (Italy). *Quat. Geochronol.* **82**, 101519 (2024).
63. Bartz, M. et al. First experimental evaluation of the alpha efficiency in coarse-grained quartz for ESR dating purposes: implications for dose rate evaluation. *Sci. Rep.* **9**, 19769 (2019).
64. Durcan, J. A., King, G. E. & Duller, G. A. T. DRAC: dose rate and age calculator for trapped charge dating. *Quat. Geochronol.* **28**, 54–61 (2015).
65. Prescott, J. R. & Hutton, J. T. Cosmic ray and gamma ray dosimetry for TL and ESR. *Int. J. Radiat. Appl. Instrumentation. Part D. Nucl. Tracks Radiat. Meas.* **14**, 223–227 (1988).
66. Prescott, J. R. & Hutton, J. T. Cosmic ray contributions to dose rates for luminescence and ESR dating: large depths and long-term time variations. *Radiat. Meas.* **23**, 497–500 (1994).

67. Blott, S. J. & Pye, K. Gradistat: a grain size distribution and statistics package for the analysis of unconsolidated sediments. *Earth Surf. Process. Landf.* **26**, 1237–1248 (2001).
68. Caratini, C. & Guinet, P. *Pollen et Spores d'Afrique Tropicale* (CNRS, 1974).
69. Ybert, J. *Atlas de Pollens de Cote d'Ivoire* (Office de la Recherche Scientifique et Technique Outre-Mer, 1979).
70. Gosling, W. D., Miller, C. S. & Livingstone, D. A. Atlas of the tropical West African pollen flora. *Rev. Palaeobot. Palynol.* **199**, 1–135 (2013).
71. Fick, S. E. & Hijmans, R. J. WorldClim 2: new 1-km spatial resolution climate surfaces for global land areas. *Int. J. Climatol.* **37**, 4302–4315 (2017).
72. Allsworth-Jones, P. *The Middle Stone Age of Nigeria in its West African Context* (Archaeopress Publishing Ltd).

Acknowledgements This paper is dedicated to the memory of V. P. Lioubin who passed away in 2018. We thank Lioubin's widow, E. Belyaeva, for her support of this work. All authors thank the Institut d'Histoire, d'Art et d'Archéologie de l'Afrique (IHAAA, Abidjan), the Institut des Sciences Anthropologiques de Développement (Abidjan) and the Université Félix Houphouët Boigny (Abidjan) for their huge logistical and administrative support during the fieldwork. We also thank the Max Planck Society's Human Palaeosystems Group and the Leakey Foundation (grant no. Fall 201910115) for their financial support (to the principal investigator, E.M.L.S.). E.BA.'s postdoctoral research received funding from the Fyssen Foundation, the Max Planck Society (Human Palaeosystems Group) and the European Union's Horizon 2020 research and innovation programme under Marie Skłodowska-Curie grant agreement no. 101107408. M.D.'s research is currently supported by the Spanish State Research Agency (AEI), through (1) a Ramón y Cajal Fellowship RYC2018-025221-I funded by MCIN/AEI/10.13039/501100011033/ 'ESF Investing in your future', and (2) grant PID2021-123092NB/-C22 funded by MCIN/AEI/ 10.13039/501100011033/'ERDF A way of making Europe'. K.N. has received funding from the European Union's Horizon 2020 research and innovation programme under Marie Skłodowska-Curie grant agreement no. 1010227259. Financial support for the ESR dating was provided by the Access to Research Infrastructures activity in the Horizon 2020 programme of the European Union (IPERION HS grant agreement no. 871034). We are grateful to H. Groucutt for providing feedback on an earlier draft of this manuscript and A. Leplongeon for her valuable comments. We also thank C. Tribolo and N. Mercier for performing and helping with the high-resolution gamma spectrometry analyses at Archeoscience Bordeaux, and R. Ashurst from the University of Sheffield for preparing the OSL and ESR dating samples. We also thank University of South Florida IASCE Paleoecology laboratory members B. Huebner, J. Jean-Baptiste, L. Koerner, A. Malerba, J. Rogers and O. Young for their help preparing the pollen samples. We additionally thank J. Kutowsky for helping with sample import/shipment permits. We thank M. O'Reilly and H. Sell for formatting the illustrations. All authors also thank all the students, G. Kassi, K. Desire Dongo and G. Kouassi, for their presence and participation in the Anyama fieldwork seasons.

Author contributions The project was conceived and directed by E.M.L.S., and implemented by E.M.L.S., E.BA., J.A.B., K.N. and C.D.N. J.A.B. led the excavations and performed cleaning and sampling. E.H., J.N.C., K.N., E.BA., E.A.K. and E.L. assisted J.A.B. with the excavations and sample recovery. F.Y.G. provided advice, guidance and help with the sampling. J.A.B. managed the sedimentological analyses. E.BA., M.D.B., M.D. and M.J.A.E. conducted the chronological analyses. S.E. conducted the phytolith analyses and C.K. conducted the pollen analyses. P.R., R.P., J.I. and E.S. conducted the bulk sediment isotope and biomarker analyses. E.BA., J.A.B. and E.M.L.S. coordinated and led the writing of the paper. E.BA., J.A.B. and A.F.B. were responsible for drawing and compiling the illustrations.

Funding Open access funding provided by Max Planck Society.

Competing interests The authors declare no competing interests.

Additional information

Supplementary information The online version contains supplementary material available at https://doi.org/10.1038/s41586-025-08613-y.

Correspondence and requests for materials should be addressed to Eslem Ben Arous, James A. Blinkhorn or Eleanor M. L. Scerri.

Peer review information *Nature* thanks Jean-Jacques Bahain, William Rink, Richard Roberts, Kira Westaway and the other, anonymous, reviewer(s) for their contribution to the peer review of this work.

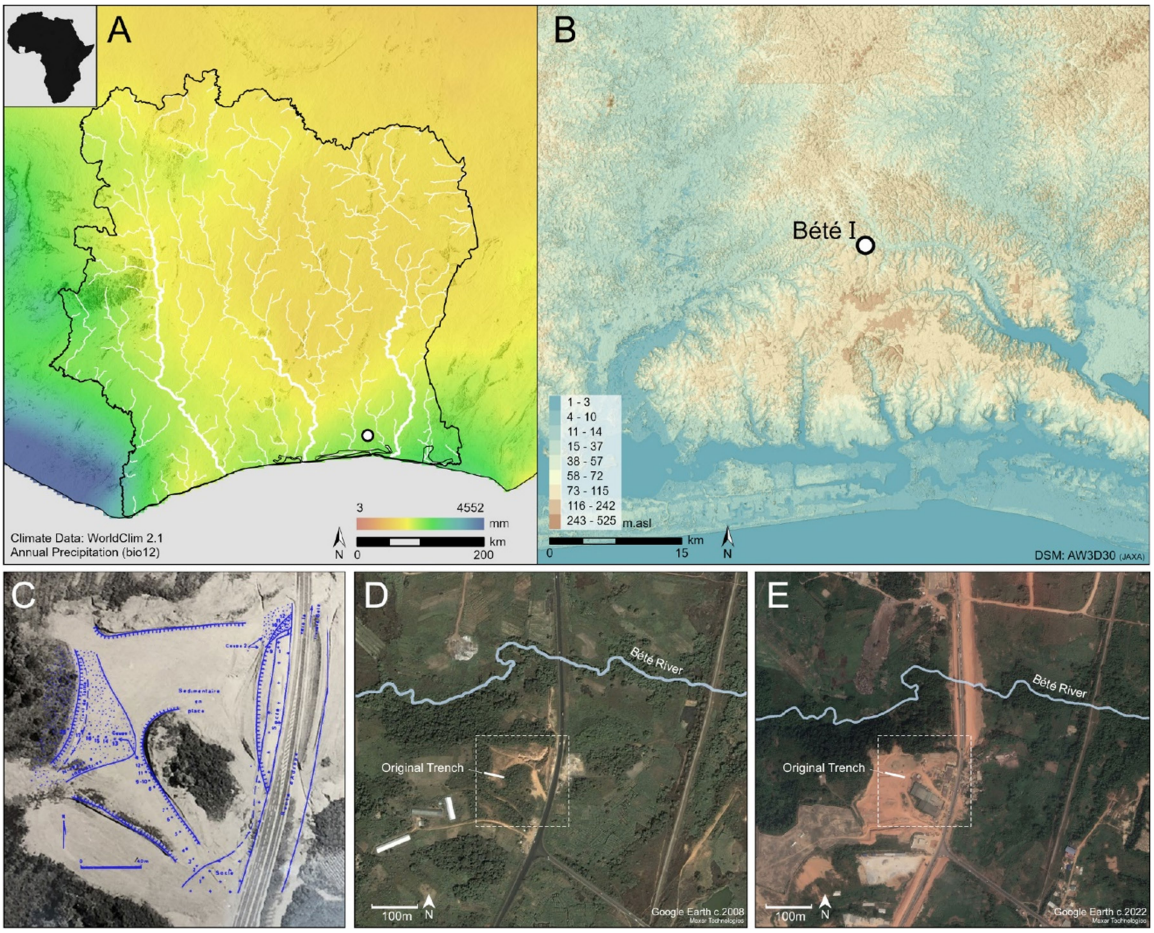

Extended Data Fig. 1 | Location and details of quarry site at Anyama. A, Map of Côte d'Ivoire, showing modern annual precipitation[71] and river systems. **B**, Digital surface model showing location of Bété I within the wider region. **C**, Historical aerial imagery of the Anyama Quarry with Bété I sequence (c.1980s, courtesy of F.Y.G.) with site plan[72] showing trench locations. **D**, Google Earth imagery from 04/2008, showing conditions at the site and the Bété River, and **E**, imagery from 01/2022, showing the expansion of the quarry and subsequent destruction of the site.

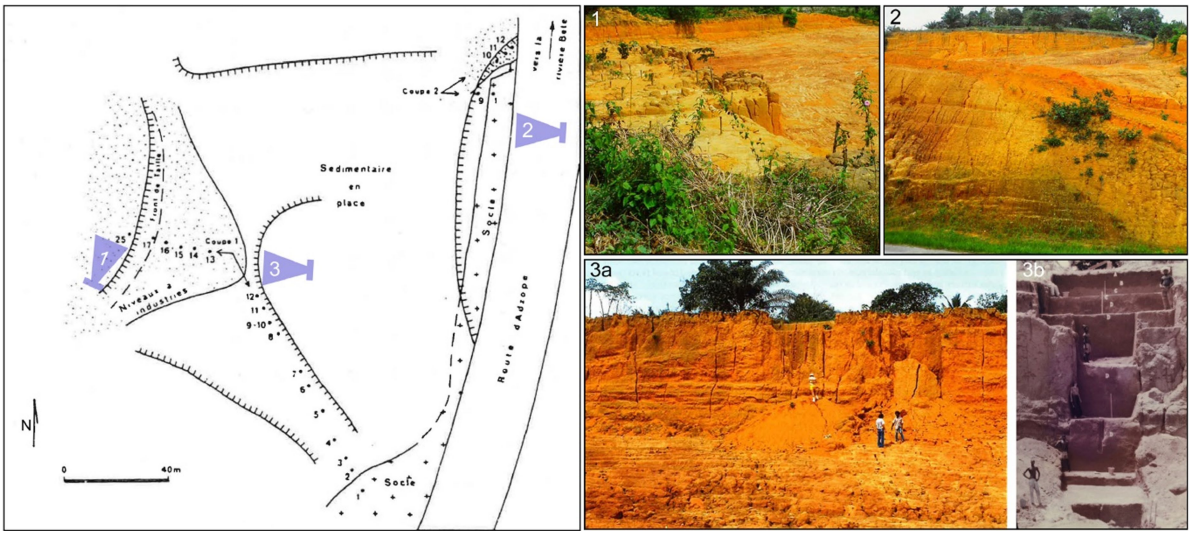

Extended Data Fig. 2 | Historical photos of excavations at Bété I. See SI-1 for details. **1**–**3a**, Photos of Bété I in November 1983 taken by P. Allsworth-Jones during a visit to the site, and **3b**, photo of main trench at Bété I during excavation in 1990s (courtesy of F.Y.G.).

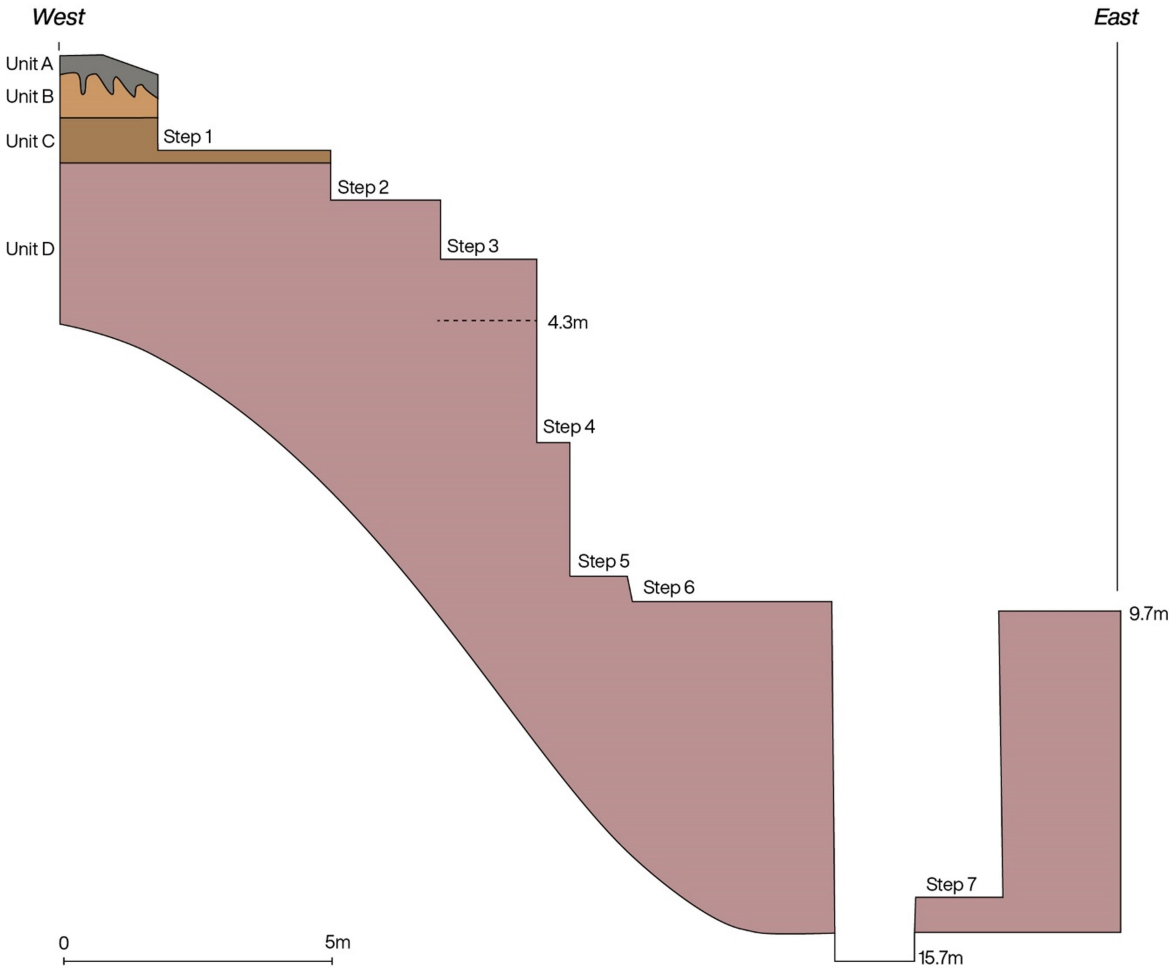

Extended Data Fig. 3 | Historical longitudinal section across the Bété I excavation. Longitudinal section across the Bété I excavation area (Steps 1–3), and the cleaned Quarry wall (Steps 4–6) and Test Pit 1 (Step 7), redrawn from Figure 6 in ref. 21, differentiating the Terre de Barre deposits of Units A-D and highlighting the steps re-examined in this study (Steps 1–4) and the lowermost artefact bearing level at 4.3 m.

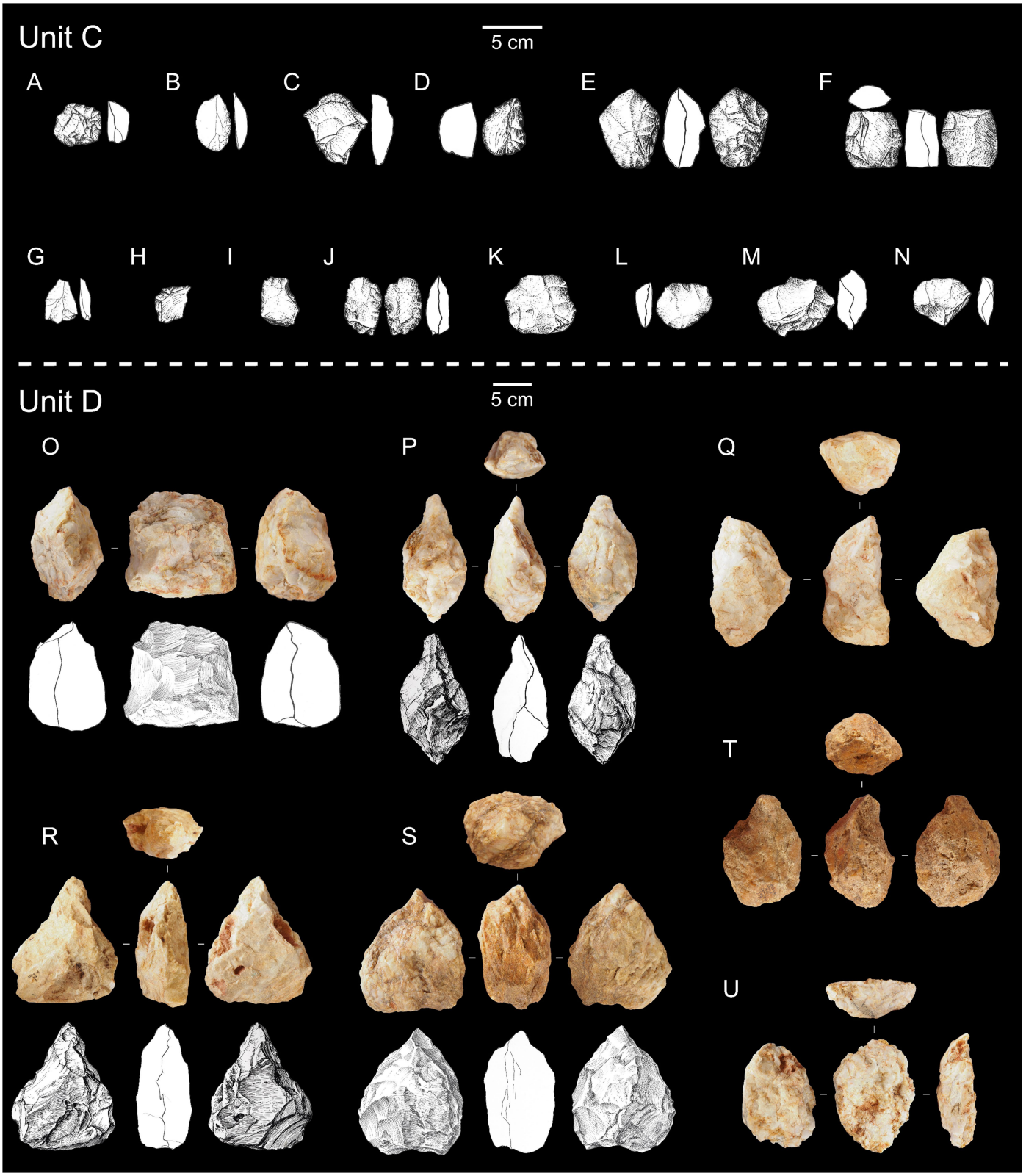

Extended Data Fig. 4 | Stone tools from Units C and D at Bété I and III from ref. 21, and photos taken of the remaining artefact collection at the Institut des Sciences Anthropologiques de Développement (ISAD) in 2021. Unit C: **A**, 'end-scraper'; **B**, 'point'; **C**, 'end-scraper à museau'; **D**, 'double-ended carinated end-scraper'; **E**, 'small handaxe'; **F**, 'fragment of a bifacial foliate piece'; **G**, 'point Levallois'; **H**, 'combination tool'; **I**, 'end-scraper with spine'; **J**, 'short foliate biface'; and **K**-**N**, 'cores'. Unit D: **O**, 'side and end chopper'; **P**, 'biface - trihedral'; **Q**, bifacial LCT (our term); **R**, 'pick with double-flat cross-section of the body and centred quadrihedral distal point'; **S**, 'pick with double-flat cross section of the body and centred trihedral distal point'; **T**–**U**, bifacial pieces (our term). **A**-**N** and **O**,**P**,**R**,**S** are from ref. 21.

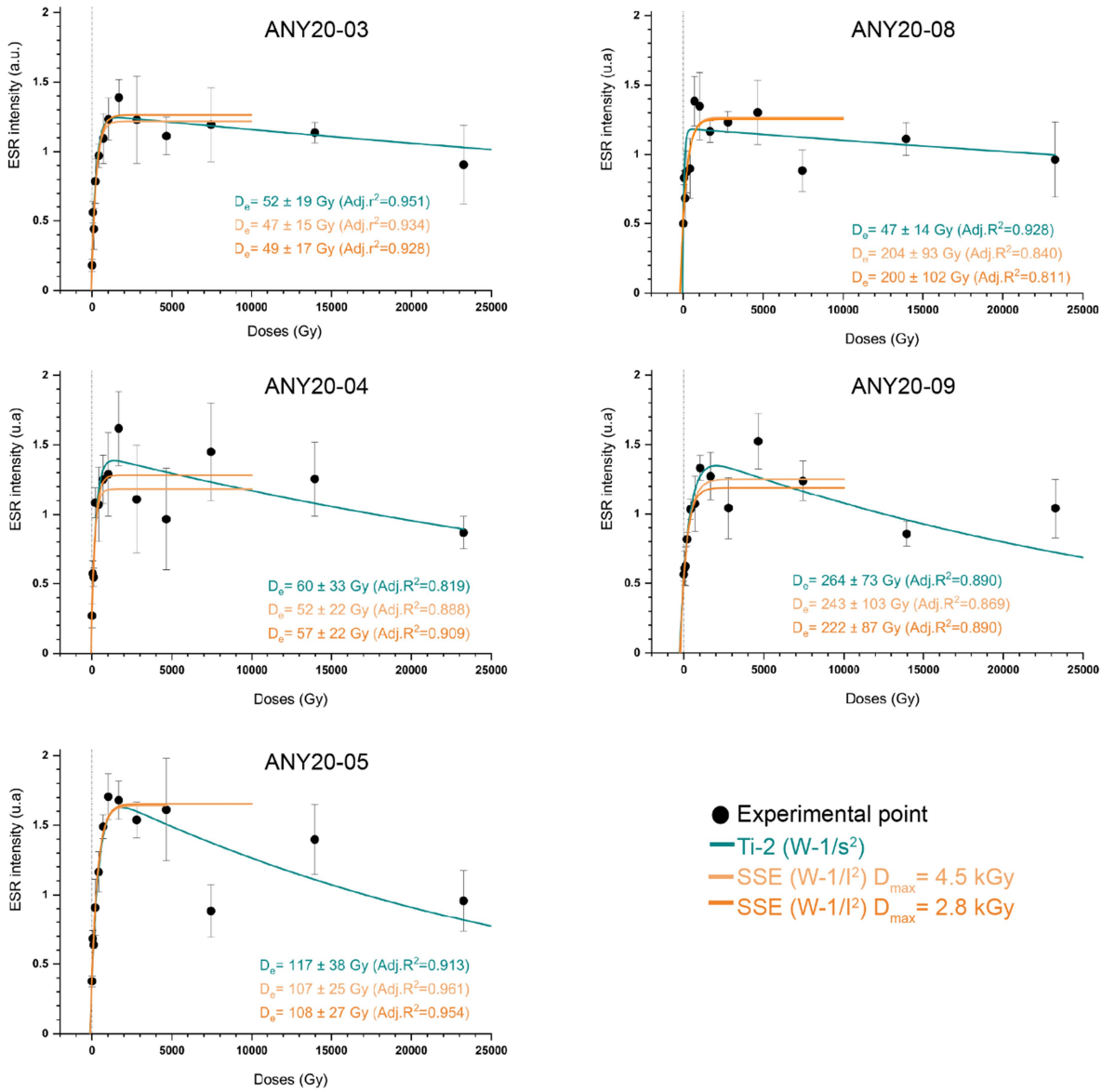

Extended Data Fig. 5 | ESR dose response curves (DRCs) derived from the Ti-H ESR signal measured in the quartz samples from Bété I. Fitting was performed as follows: (see text for further information): **a**, with the Ti-2 function (data weighting by $1/s^2$); **b**, with the single saturating exponential (SSE) function (data weighting by $1/I^2$) with D_{max} = 4.5 kGy; and **c**, D_{max} = 2.8 kGy. Each experimental data point and associated vertical errors bar represent the mean ESR intensity and 1 standard deviation derived from the repeated measurements, respectively. DRCs display ESR intensities after noise subtraction.

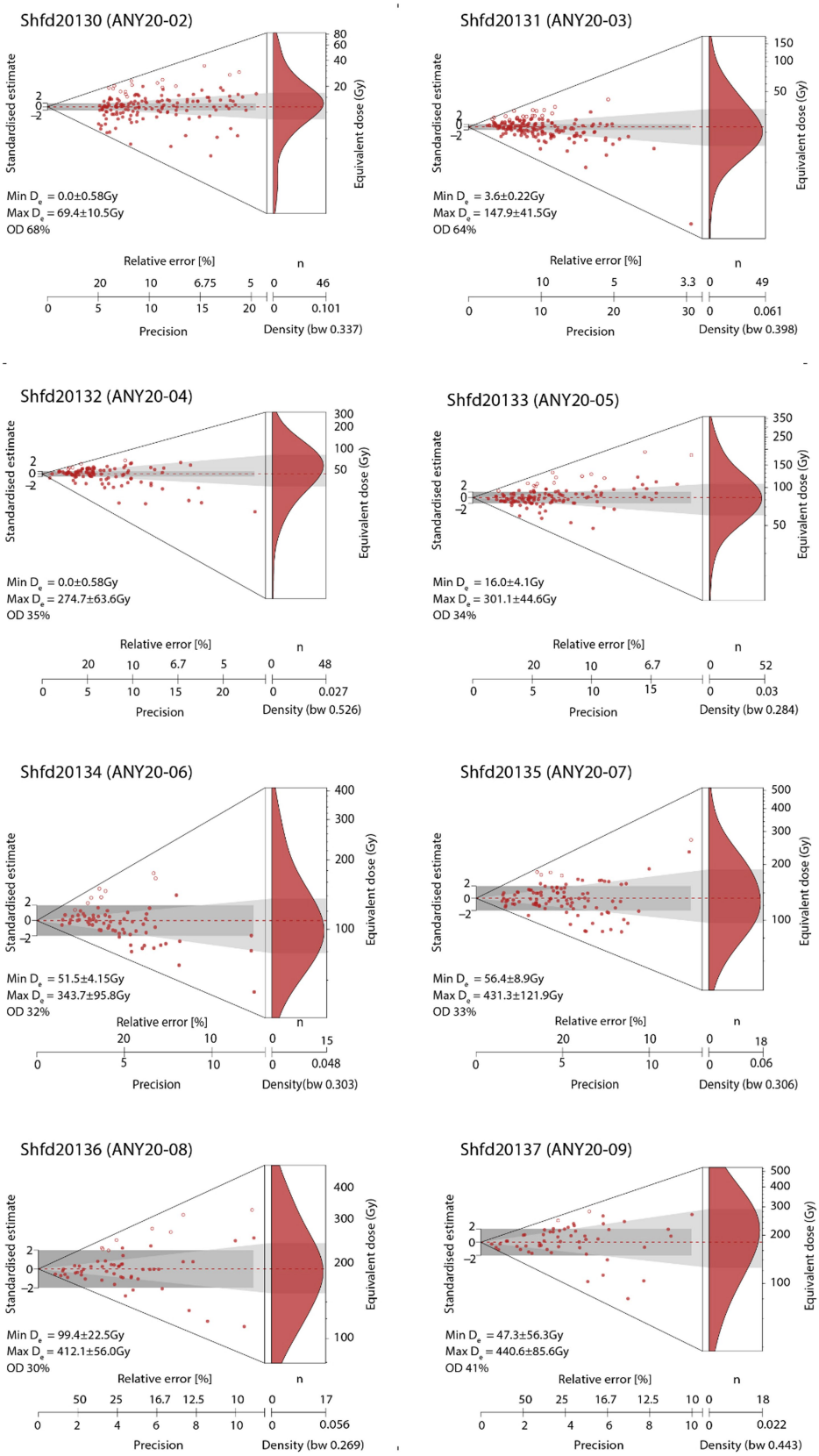

Extended Data Fig. 6 | Abanico plots of D_e replicate single grain (SG) OSL data centred on the Central Age Model D_e also used for age calculation purposes. Open circles indicate aliquots considered as outliers (see SI-3 for details). Overdispersion (OD) as shown is prior to outlier removal and grey bar shows the 2 standard error estimate on the Central Age D_e.

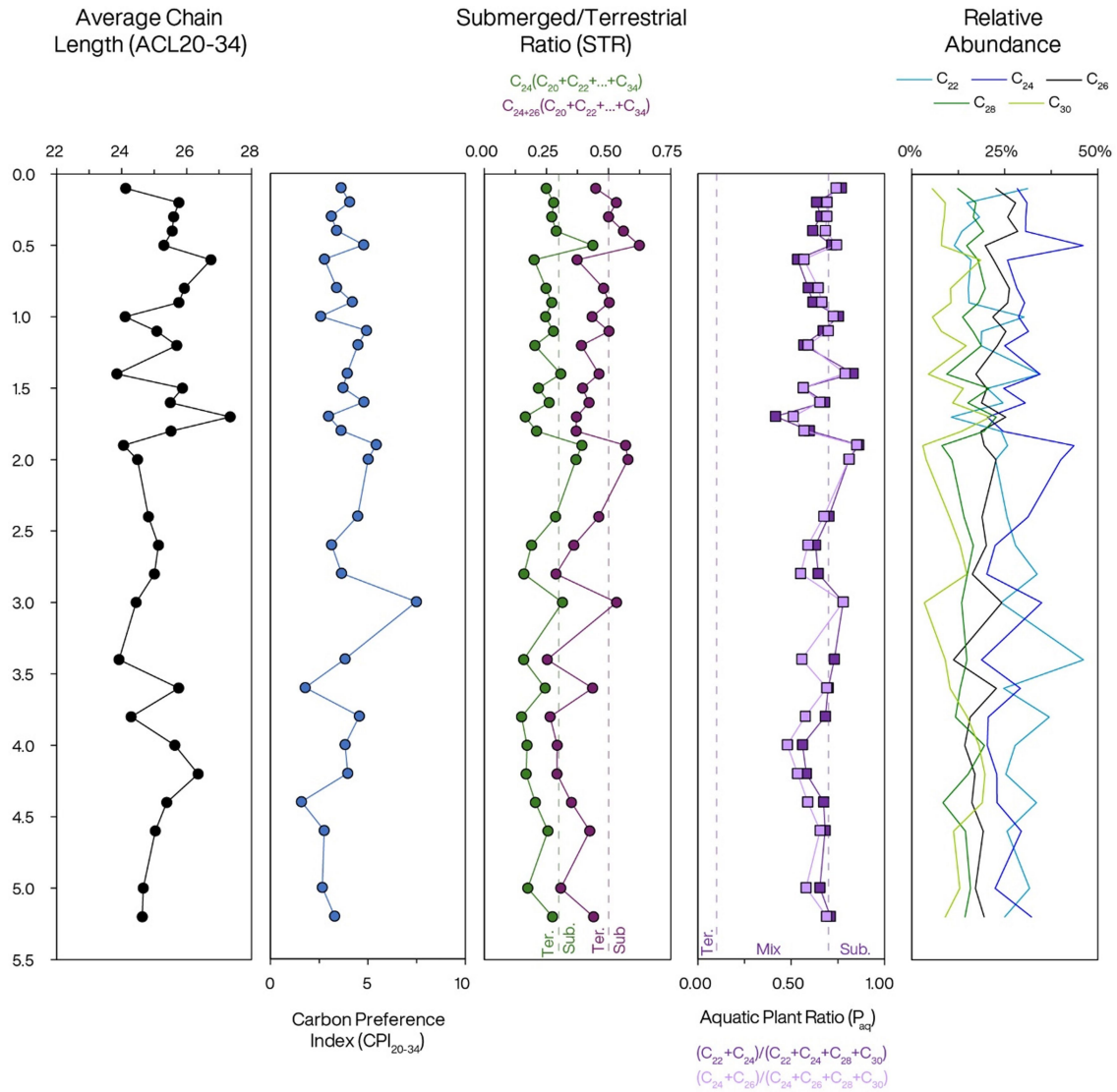

Extended Data Fig. 7 | Biomarker signatures of the Bété I archaeological sediments. See Section 4.2.1 for ACL and CPI calculations. Two versions of the submerged/terrestrial ratio were calculated: STR24 and STR24 + 26. Submerged aquatic plants tend to have values greater than 0.25 and 0.50 for STR24 and STR24 + 26, respectively. Two versions of the aquatic plant ratio (P_{aq}) were also calculated to compare with STR. Terrestrial plants typically have sedimentary P_{aq} values of less than 0.1 while aquatic plants tend to have values greater than 0.7. Values ranging between 0.1 and 0.7 typically represent a mixed input that includes terrestrial, emergent, and aquatic plants. The percentages of compound abundances are relative to the dominant FAMEs (C22 + C24 + C26 + C28 + C30). Higher values reflect relatively increased inputs of the respective compounds.

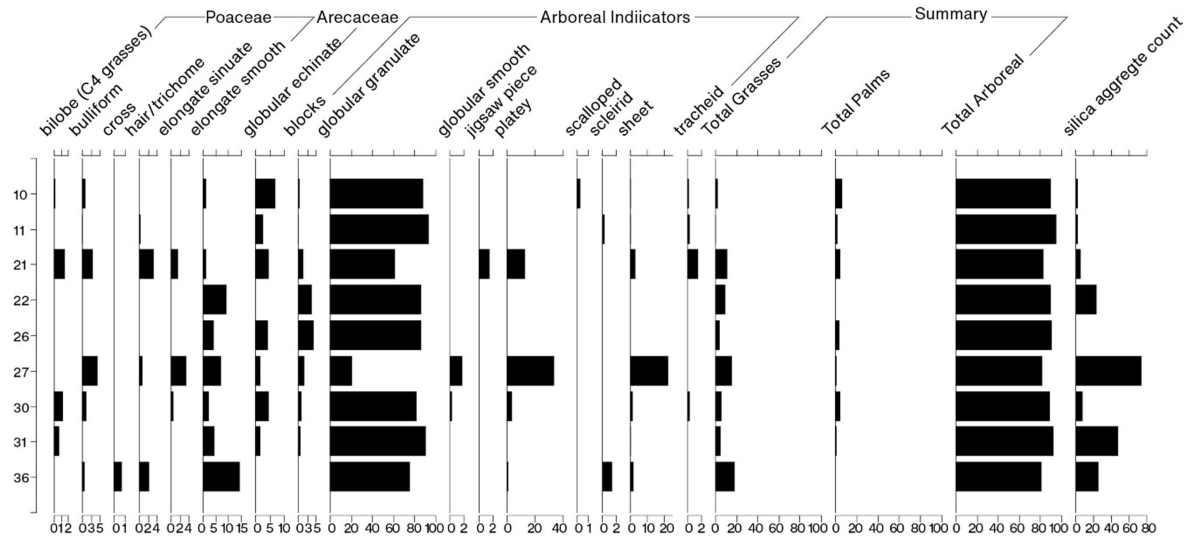

Extended Data Fig. 8 | C2 diagram of percentages of phytoliths types. Samples 21, 22, 26, 27 and 36 are calculated on phytolith counts below the statistically viable minimum number of recorded phytoliths so their interpretation should be treated with caution.

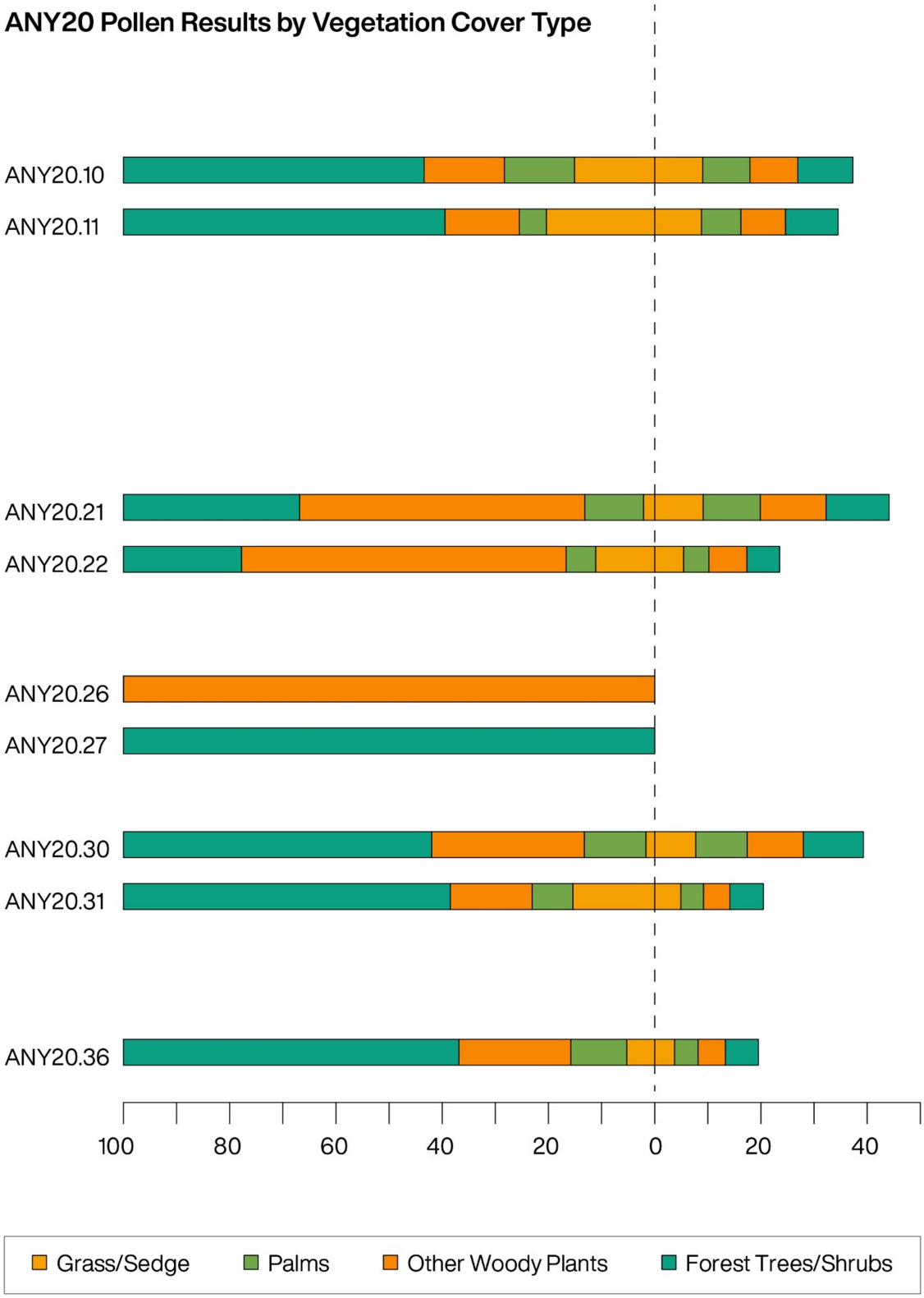

Extended Data Fig. 9 | Barplot showing proportional representation of key groups of pollen (left) and log values of pollen concentrations (right). Note that samples 26 and 27 do not have sufficient pollen concentrations to produce meaningful proportions.

nature portfolio

Corresponding author(s): Eslem BEN AROUS, James. A. BLINKHORN, E. SCERRI

Last updated by author(s): Dec 13, 2024

Reporting Summary

Nature Portfolio wishes to improve the reproducibility of the work that we publish. This form provides structure for consistency and transparency in reporting. For further information on Nature Portfolio policies, see our Editorial Policies and the Editorial Policy Checklist.

Statistics

For all statistical analyses, confirm that the following items are present in the figure legend, table legend, main text, or Methods section.

n/a	Confirmed
☐	☒ The exact sample size (*n*) for each experimental group/condition, given as a discrete number and unit of measurement
☒	☐ A statement on whether measurements were taken from distinct samples or whether the same sample was measured repeatedly
☒	☐ The statistical test(s) used AND whether they are one- or two-sided *Only common tests should be described solely by name; describe more complex techniques in the Methods section.*
☒	☐ A description of all covariates tested
☒	☐ A description of any assumptions or corrections, such as tests of normality and adjustment for multiple comparisons
☐	☒ A full description of the statistical parameters including central tendency (e.g. means) or other basic estimates (e.g. regression coefficient) AND variation (e.g. standard deviation) or associated estimates of uncertainty (e.g. confidence intervals)
☐	☒ For null hypothesis testing, the test statistic (e.g. *F*, *t*, *r*) with confidence intervals, effect sizes, degrees of freedom and *P* value noted *Give P values as exact values whenever suitable.*
☒	☐ For Bayesian analysis, information on the choice of priors and Markov chain Monte Carlo settings
☒	☐ For hierarchical and complex designs, identification of the appropriate level for tests and full reporting of outcomes
☒	☐ Estimates of effect sizes (e.g. Cohen's *d*, Pearson's *r*), indicating how they were calculated

Our web collection on statistics for biologists contains articles on many of the points above.

Software and code

Policy information about availability of computer code

Data collection	ESR data : Bruker WINEPR system v2.22; Microcal OriginPro v2022b; OSL data : Analyst v.4.57; R Statistical Software (v4.2.2) with RLumShiny (v1.8.1.1) and Luminescence v 0.9.26 R code packages; Pollen data : R studio v4.2.2 and 'wesanderson' package v0.3.6; Pytholiths data : C2 v1.8.0; Sedimentology data : Gradistat v8; Biomarker data: PAST 4.03 statistical software; MassHunter Qualitative Analysis v.8.0 Map : ArcMap v10.5; BartSoft v4.2;
Data analysis	The data analysis (dating, sedimentology, istopics and biomarkers) are precisely described and provided in the Supplementary Information, Methods online and Extended Data Figures.

For manuscripts utilizing custom algorithms or software that are central to the research but not yet described in published literature, software must be made available to editors and reviewers. We strongly encourage code deposition in a community repository (e.g. GitHub). See the Nature Portfolio guidelines for submitting code & software for further information.

Data

Policy information about availability of data

All manuscripts must include a data availability statement. This statement should provide the following information, where applicable:

- Accession codes, unique identifiers, or web links for publicly available datasets
- A description of any restrictions on data availability
- For clinical datasets or third party data, please ensure that the statement adheres to our policy

Provide your data availability statement here.

Research involving human participants, their data, or biological material

Policy information about studies with human participants or human data. See also policy information about sex, gender (identity/presentation), and sexual orientation and race, ethnicity and racism.

Reporting on sex and gender	NA
Reporting on race, ethnicity, or other socially relevant groupings	NA
Population characteristics	NA
Recruitment	NA
Ethics oversight	NA

Note that full information on the approval of the study protocol must also be provided in the manuscript.

Field-specific reporting

Please select the one below that is the best fit for your research. If you are not sure, read the appropriate sections before making your selection.

☐ Life sciences ☐ Behavioural & social sciences ☒ Ecological, evolutionary & environmental sciences

For a reference copy of the document with all sections, see nature.com/documents/nr-reporting-summary-flat.pdf

Ecological, evolutionary & environmental sciences study design

All studies must disclose on these points even when the disclosure is negative.

Study description	We report a clear association between late Middle Pleistocene material culture and a wet tropical forest in southern Côte d'Ivoire. Twinned Optically Stimulated Luminescence (OSL) and Electron Spin Resonance (ESR) dating methods constrain the onset of human occupations at Bété I to ~150 ka. Plant wax biomarker, stable isotope, phytolith and pollen analyses of associated sediments all point to a wet forest environment.
Research sample	Sediment samples from Bété I site used to generate chronometric dates (SA and SG ages : 8; Ti-H ESR ages : 5), 37 sediments characterized, 37 bulk isotopes analysis, 31 sediments for plant wax analyses, 9 sediments for phytoliths and pollen
Sampling strategy	Sediment sampled to cover the first ca. 6m of the sedimentary sequence of Bété I.
Data collection	Fieldtrip in March 2020.
Timing and spatial scale	Not relevant.
Data exclusions	*If no data were excluded from the analyses, state so OR if data were excluded, describe the exclusions and the rationale behind them, indicating whether exclusion criteria were pre-established.*
Reproducibility	Not relevant.
Randomization	Not relevant.
Blinding	Not applicable to palaeontology/archaeology.

Did the study involve field work? ☒ Yes ☐ No

Field work, collection and transport

Field conditions	Bété I is located in the present-day tropical forest and excavations in March 2020 (hot and humid).
Location	Anyama city, ca. 20 km North of Abidjan.
Access & import/export	*Describe the efforts you have made to access habitats and to collect and import/export your samples in a responsible manner and in compliance with local, national and international laws, noting any permits that were obtained (give the name of the issuing authority, the date of issue, and any identifying information).*
Disturbance	*Describe any disturbance caused by the study and how it was minimized.*

Reporting for specific materials, systems and methods

We require information from authors about some types of materials, experimental systems and methods used in many studies. Here, indicate whether each material, system or method listed is relevant to your study. If you are not sure if a list item applies to your research, read the appropriate section before selecting a response.

Materials & experimental systems

n/a	Involved in the study
☒	☐ Antibodies
☒	☐ Eukaryotic cell lines
☐	☒ Palaeontology and archaeology
☒	☐ Animals and other organisms
☒	☐ Clinical data
☒	☐ Dual use research of concern
☒	☐ Plants

Methods

n/a	Involved in the study
☒	☐ ChIP-seq
☒	☐ Flow cytometry
☒	☐ MRI-based neuroimaging

Palaeontology and Archaeology

Specimen provenance	NA
Specimen deposition	NA
Dating methods	Optically Stimulated Method (OSL) and Electron Spin Resonance (ESR) on quartz

☐ Tick this box to confirm that the raw and calibrated dates are available in the paper or in Supplementary Information.

Ethics oversight	No ethical approval was required

Note that full information on the approval of the study protocol must also be provided in the manuscript.

Plants

Seed stocks	NA
Novel plant genotypes	NA
Authentication	NA